Applied Physics Letters

Resistive detection of the Néel temperature of Cr_2O_3 thin films

Cite as: Appl. Phys. Lett. **114**, 022402 (2019); https://doi.org/10.1063/1.5082220
Submitted: 20 November 2018 • Accepted: 01 January 2019 • Published Online: 15 January 2019

Tatsuya Iino, Takahiro Moriyama, Hiroyuki Iwaki, et al.

AIP Publishing

Applied Physics Letters ARTICLE scitation.org/journal/apl

Resistive detection of the Néel temperature of Cr_2O_3 thin films

Cite as: Appl. Phys. Lett. **114**, 022402 (2019); doi: 10.1063/1.5082220
Submitted: 20 November 2018 · Accepted: 01 January 2019 · Published Online: 15 January 2019

Tatsuya Iino,[1] Takahiro Moriyama,[1,a)] Hiroyuki Iwaki,[1] Hikaru Aono,[2] Yu Shiratsuchi,[2] and Teruo Ono[1]

AFFILIATIONS

[1] Institute for Chemical Research, Kyoto University, Gokasho, Uji, Kyoto 611-0011, Japan
[2] Graduate School of Engineering, Osaka University, Suita, Osaka 565-0871, Japan

[a)] mtaka@scl.kyoto-u.ac.jp

ABSTRACT

Although bulk magnetic properties of various antiferromagnets have been vigorously studied since long ago, their properties in the form of thin films, which are more relevant to antiferromagnetic spintronic devices, have not been investigated as much. In this work, we characterized the Néel temperature of Cr_2O_3 thin films by investigating the temperature dependence of the spin Hall magnetoresistance in Cr_2O_3/Pt bilayers. A precise determination of the Néel temperature was made possible by carefully designing the direction of the magnetic anisotropy in Cr_2O_3. The results provide a reliable way to determine the Néel temperature of antiferromagnetic thin films.

Recent pioneering explorations of spintronic phenomena in antiferromagnetic materials such as magnetoresistance,[1,2] spin torque effect,[3–7] and spin current transmissivity[8–10] have been accelerating active research in antiferromagnetic spintronics.[11,12] Antiferromagnets, used to be regarded as useless materials, are now expected to yield novel spintronic applications, such as THz devices and magnetic field proof memory devises, by taking advantage of the unique properties of antiferromagnets; i.e., the fast dynamics and zero magnetization in antiferromagnets.

There are a wide variety of material choices for antiferromagnets from insulator to metals and from single elements to alloys and ionic crystals.[11,12] Although bulk magnetic properties of various antiferromagnets have been vigorously studied since the 1950s after the Néel's antiferromagnetic theory was introduced, their properties in the form of thin films and nanostructures, which are relevant to the spintronic devices, have not been investigated as much. Since a finite size effect on magnetic properties in antiferromagnets can be as significant as that in ferromagnets,[13–15] it is important and crucial to investigate the properties of antiferromagnetic thin films, such as the magnetic anisotropy and the Néel temperature T_N.

A number of recent reports suggest that magnetoresistive measurements can be a convenient method for characterizing antiferromagnetic thin films[1,2,7] while traditional techniques, such as conventional magnetometry techniques, μSR,[16,17] neutron diffraction,[18] and X-ray magnetic linear dichroism (XMLD),[19,20] are often unsuitable for thin film characterization because they require sufficient interaction cross sections, or volume. In particular, the spin Hall magnetoresistance (SMR) has been found versatile to probe a variety of antiferromagnetic thin film materials.[21–24] SMR generally emerges in a multilayer having an interface between a magnetic material and a spin Hall material (such as Pt, Ta, and W). Upon the electrical current flow, the interaction between the magnetic moments and the spin current injected into the magnetic material from the spin Hall material gives rise to the magnetoresistance. The resistance R essentially varies depending on the relative orientation between the direction of the current flow **i** and the magnetization direction **m** by[24]

$$R = R_0 - \Delta R \sin^2(\angle(\mathbf{i}, \mathbf{m})), \tag{1}$$

where R_0 is the magnetization independent contribution to the resistance and ΔR represents the resistance change due to SMR. One can therefore identify the orientation of magnetic moments by referencing the resistance change. SMR was first discovered with a $Y_3Fe_5O_{12}$/Pt bilayer system[25,26] and was later proved effective even for identifying the Néel vector orientation in antiferromagnets[7,21–24] where **m** in Eq. (1) can be taken as the microscopic magnetic moments in the antiferromagnet.

By taking advantage of SMR, a few groups have now claimed to capture the magnetic phase transition in antiferromagnets.[23,24] Cr_2O_3 is one of the ideal materials for such experiments because it has a uniaxial magnetic anisotropy so that it is relatively easy to define its antiferromagnet state. They observe that the magnetoresistance in the Cr_2O_3/Pt bilayer increases above the Néel temperature. However, this is totally the opposite trend when considering a common variation of the magnetic susceptibility in the vicinity of the Néel temperature, i.e., the magnetic susceptibility in their configuration should be smaller above the Néel temperature and therefore smaller magnetoresistance should be expected. It is an open question if the observed SMR is due to a consequence of the antiferromagnetic-paramagnetic transition of the whole film or due only to the contribution of the proximity magnetization at the Cr_2O_3/Pt interface. As the precise determination of the Néel temperature of antiferromagnetic thin films would be greatly desirable, it is important to further explore and interpret the temperature dependence of SMR in antiferromagnet/spin Hall material bilayers.

In this work, we investigated the temperature dependence of SMR in two different epitaxially grown Cr_2O_3 (0001)/Pt and Cr_2O_3 ($10\bar{1}0$)/Pt samples in which the magnetic anisotropy lies out of the sample plane and in the plane, respectively. While we obtained a temperature dependence of SMR in α-Al_2O_3 (0001) sub./Cr_2O_3 (0001)/Pt consistent with the previous work, that of SMR in α-Al_2O_3 ($10\bar{1}0$) sub./Cr_2O_3 ($10\bar{1}0$)/Pt behaves differently and captures better the Néel temperature of the Cr_2O_3.

Cr_2O_3 20 nm/Pt 2 nm bilayers were grown by magnetron sputtering on a single crystal α-Al_2O_3 substrate. The Cr_2O_3 layer was deposited at 773 K by means of a reactive sputtering technique in an Ar + O_2 gas mixture. More detailed fabrication processes can be found elsewhere.[27] α-Al_2O_3 (0001) and α-Al_2O_3 ($10\bar{1}0$) were chosen so that a desired epitaxial orientation of the hexagonal crystalline Cr_2O_3 can be promoted [Fig. 1(a)]. Reflective high-energy electron diffraction (RHEED) images after the deposition of Cr_2O_3 shown in Figs. 1(b) and 1(c) indicate that the films grown on the α-Al_2O_3 (0001) and α-Al_2O_3 ($10\bar{1}0$) substrates have a crystalline orientation relationship of α-Al_2O_3(0001) [$\bar{2}110$]//Cr_2O_3(0001) [$\bar{2}110$] and α-Al_2O_3($10\bar{1}0$) [0001]//Cr_2O_3($10\,\bar{1}\,0$) [0001], respectively. The Pt layer was then deposited on top of the Cr_2O_3 layer at room temperature. From now on, α-Al_2O_3(0001)/Cr_2O_3(0001)/Pt is called the C-plane sample and α-Al_2O_3($10\bar{1}0$)/Cr_2O_3($10\bar{1}0$)/Pt is called the M-plane sample according to the general conventions for hexagonal crystals.

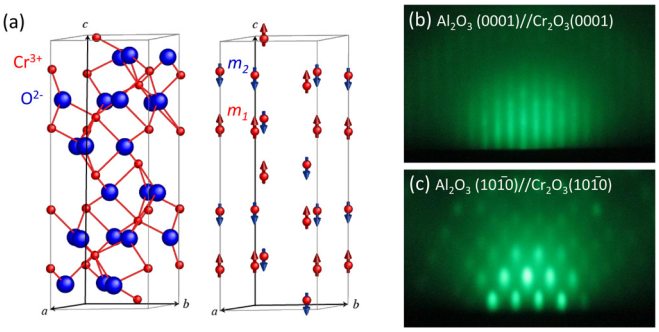

FIG. 1. (a) Schematic illustration of the Cr_2O_3 crystal structure and the magnetic structure. (b) [$11\bar{2}0$] Azimuth RHEED pattern of the Cr_2O_3 surface in the C-plane sample. (c) [0001] Azimuth RHEED pattern of the Cr_2O_3 surface in the M-plane sample.

Magnetoresistance measurements were performed on the photolithographically patterned cross structure shown in Fig. 2(a). We employed the ratio measurement technique to capture a small change in the resistance.[2] As shown in Fig. 2(a), the voltages on two different branches V_1 (between the electrodes 1 and 3) and V_2 (between the electrodes 2 and 3) were measured while a d.c. current was applied between electrodes 1 and 2. We used a nanovoltmeter (Keithley Nano-voltmeter 2182A) to take V_1, V_2, and V_1/V_2, which are translated to the resistances R_1, R_2, and R_1/R_2, as functions of temperature T and external field H. Temperature was scanned in the range of 250–350 K which covers the expected Néel temperature of the Cr_2O_3 ($T_N = 307$ for the bulk[28]). The external field up to 9 Tesla was applied along the branch on which V_1 was measured.

The hexagonal Cr_2O_3 possesses a magnetic easy axis along the c-axis (or [0001] direction) as the magnetic structure shown in Fig. 1(a). Therefore, below the Néel temperature T_N, $T < T_N$, and in the ground state, the Néel vector in the C-plane sample points perpendicular to the sample plane and the one in the M-plane sample points in the sample plane and parallel to the y-direction [see Figs. 2(a) and 2(b) with the coordinate system]. On the other hand, at $T > T_N$, the external magnetic field induces the net paramagnetic moments $\boldsymbol{m}(H)$ [see the lower panel of Fig. 2(b)]. Figures 2(c)–2(e) illustrate the orientation of the magnetic

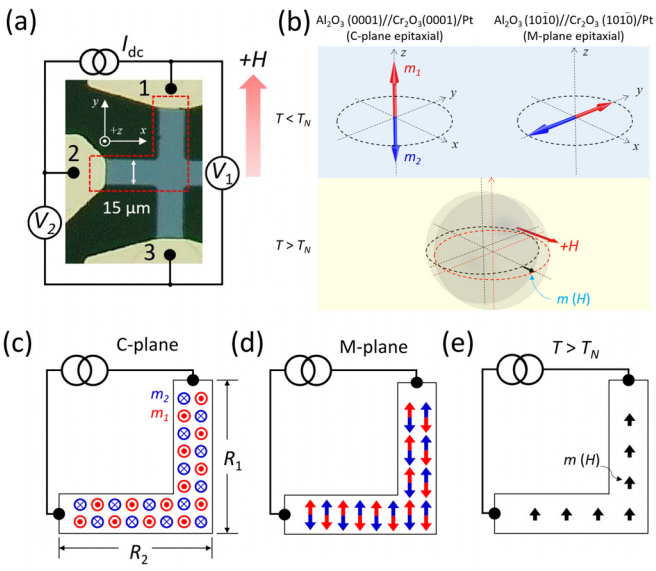

FIG. 2. (a) Microscopy image of the device under test with the electrical circuitry used in our measurements. (b) Configuration of the magnetic moments of Cr_2O_3 at $T < T_N$ and $T > T_N$. The sphere represents the random orientation of the magnetic moments in the paramagnetic state. Upon the magnetic field application, the sphere shifts to the direction of the field with the induced moment $\mathbf{m}(H)$. Schematic illustrations of (c) the C-plane and (d) the M-plane samples at $T < T_N$ with $H = 0$ T and (e) the paramagnetic state at $T > T_N$ with $H > 0$ T.

moments for the C-plane and M-plane samples with respect to the current flow with $H = 0$ T for $T < T_N$ and with respect to the induced paramagnetic moments $\mathbf{m}(H)$ by H for $T > T_N$ upon the electrical measurements.

Figure 3 shows $(R_1/R_2) - 1$ as functions of temperature and the external field for C-plane and M–plane samples. Assuming that both the branches on which R_1 and R_2 were measured are identical in length or identical in resistance, $(R_1/R_2) - 1$ should be zero. Based on the model shown in Fig. 2(c), at $T < T_N$ and with $H = 0$ T, the C-plane sample should then exhibit $(R_1/R_2) - 1 = 0$ because the relative orientation between $\mathbf{i}$ and $\mathbf{m}$ is the same for both the branches (i.e., both the branches have the same magnetoresistance contributions). On the other hand, as shown in Fig. 2(d), the M-plane sample should exhibit $(R_1/R_2) - 1 > 0$ at $T < T_N$ with $H = 0$ T because the different relative orientation between $\mathbf{i}$ and $\mathbf{m}$ [see Eq. (1)] results in a different resistance in the two branches. At $T > T_N$ with $H = 0$ T, however, $(R_1/R_2) - 1$ should be zero. It then becomes greater than zero due to the induced $\mathbf{m}(H)$ when H is increased [see Fig. 2(e)]. We note that the plots in Fig. 3 are offset by taking into account the residual $(R_1/R_2) - 1$ due to a slight difference in magnetization independent resistance. Moreover, the monotonic temperature dependence of $(R_1/R_2) - 1$ comes from the fact that the two branches are not identical in the temperature coefficient of resistance.

In the case of the C-plane sample, $(R_1/R_2) - 1$ monotonically increases with $H = 0$ T, which can be attributed to a simple temperature dependence of the magnetic independent resistance, while $(R_1/R_2) - 1$ shows a deviation from the monotonic increase with the external field [Fig. 3(a)]. The deviation starts from ~280 K which is lower than the bulk Cr_2O_3 Néel temperature, 307 K. $(R_1/R_2) - 1$ as a function of the external field shown in Fig. 3(c) indicates that the resistance smoothly varies with the field strength. The increase in $(R_1/R_2) - 1$ with increasing H above T_N is consistent with our picture described in Fig. 2(c) and mainly comes from the induced moment $\mathbf{m}(H)$ in the paramagnetic state.[24]

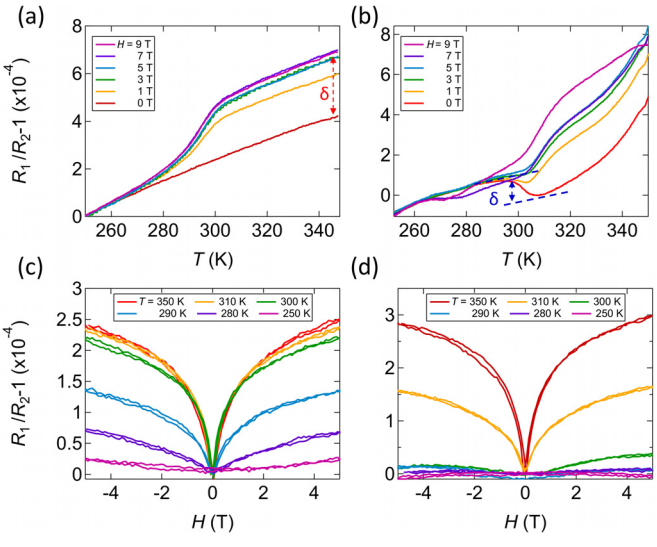

FIG. 3. Temperature dependence of $(R_1/R_2) - 1$ for (a) the C-plane sample and (b) the M-plane sample and field dependence of $(R_1/R_2) - 1$ for (c) the C-plane sample and (d) the M-plane sample.

In the case of the M-plane sample, $(R_1/R_2) - 1$ overall increases with increasing temperature but there is a significant drop at $T \sim 300$ K with $H = 0$ T. The drop is diminished as H is increased. $(R_1/R_2) - 1$ as a function of the external field shown in Fig. 3(d) also indicates that the resistance smoothly varies with the field strength above 300 K. The drop of $(R_1/R_2) - 1$ above T_N with $H = 0$ T is consistent with our model described in Figs. 2(d) and 2(e). It also explains the diminishment of the $(R_1/R_2) - 1$ drop because $(R_1/R_2) - 1$ above T_N increases with the increasing external magnetic field due to $\mathbf{m}(H)$. It should be noted that the overall temperature dependence of $(R_1/R_2) - 1$ is much more non-linear in the M-plane sample than in the C-plane sample. This might indicate that richer physics of the magnetic order in the vicinity of the Néel temperature could be captured in the M-plane samples.

We estimated the spin Hall magnetoresistance ratio $\Delta R/R_0$ for both samples from R_1/R_2 by the formula

$$\frac{\Delta R}{R_0} = \frac{2\delta}{(R_1'/R_2') + 1}, \tag{2}$$

where $R_{1,2}'$ is the magnetization independent resistance and δ is the change in R_1/R_2 upon the magnetic phase transition. Note that we assume $\delta \ll 1$ to derive the formula (see supplementary material). For the C-plane sample, δ was taken as the difference of the R_1/R_2 measured at $H = 0$ T and 5 T at $T = 350$ K as depicted in Fig. 3(a). We then found $\Delta R/R_0 = 0.026\%$ which is in good agreement with the previous reports on the same C-plane oriented Cr_2O_3/Pt.[23,24] On the other hand, for the M-plane sample, δ was taken as the R_1/R_2 drop around 300 K at $H = 0$ T as depicted in Fig. 3(b). We then obtained $\Delta R/R_0 = 0.017\%$. In the following, we discuss SMR in Cr_2O_3/Pt by comparing the C-plane and M-plane samples. There is a distinct difference in the mechanism giving rise to the SMR ratio in the C-plane and M-plane samples.

In the case of the C-plane sample, the SMR is predominantly induced by the paramagnetic $\mathbf{m}(H)$ as one can compare the magnetic states shown in Figs. 2(c) and 2(e). The antiferromagnetic moments (at $T < T_N$) seem to be robust against the external magnetic field up to 9 T[29] as one can see from Fig. 3 that $R_1/R_2 - 1$ is nearly unchanged with the external field below T_N. Moreover, it should be emphasized that one needs to apply an external field to see the magnetoresistance. Therefore, the obtained $\Delta R/R_0$ should be attributed to the SMR due to the paramagnetic Cr_2O_3.

On the other hand, in the case of the M-plane sample, the SMR is predominantly induced by the Néel vector as one can compare the magnetic states shown in Figs. 2(d) and 2(e). The advantage of the M-plane samples is that it does not require any external field to detect the Néel temperature and, therefore, the obtained Néel temperature exactly reflects the magnetic phase transition of the ground state. The obtained $\Delta R/R_0$ should represent the SMR due to the antiferromagnetic Cr_2O_3 although the magnetoresistance ratio turns out to be coincidentally very similar to the one due to the paramagnetic SMR.

Finally, we should note that the Néel temperature predicted from our measurements is smaller in the C-plane sample than in the M-plane samples. While the obtained Néel temperature for the M-plane is consistent with the bulk Cr_2O_3 value, the one for the C-plane sample seems to be reduced supposedly due to various possibilities: e.g., a proximity magnetization[30] and a crystal strain.[31] It is also possible that the application of the magnetic field could impact the ground state of the system. On the other hand, we emphasize that the measurement configuration on the M-plane samples is more robust and reliable for detecting the Néel temperature as the clear principle of the SMR detection of the Néel vector works behind the measurement.

In summary, we investigated the temperature dependence of SMR in two different epitaxially grown Cr_2O_3/Pt. While the Cr_2O_3 (0001)/Pt sample predominantly gives rise to the SMR due to paramagnetic Cr_2O_3, the Cr_2O_3 $(10\bar{1}0)$/Pt sample gives rise to the SMR due to antiferromagnetic Cr_2O_3. The SMR ratio was 0.026% for Cr_2O_3 (0001)/Pt and 0.017% for Cr_2O_3 $(10\bar{1}0)$/Pt. We capture the Néel temperature by the sudden change in the resistance as a function of temperature in both samples. Considering the mechanism giving rise to the resistance change in our measurements, Cr_2O_3 $(10\bar{1}0)$/Pt samples in which the Néel vector lies in the sample plane provide more precisely the Néel temperature. The present magnetoresistive detection scheme for determining the Néel temperature can surely apply to other antiferromagnets.

See supplementary material for the derivation of Eq. (2).

This work was supported by JSPS KAKENHI Grant Nos. 17H04924, 17H05181, 17K18991, and 15H05702.

REFERENCES

[1]X. Marti, I. Fina, C. Frontera, J. Liu, P. Wadley, Q. He, R. J. Paull, J. D. Clarkson, J. Kudrnovský, I. Turek, J. Kuneš, D. Yi, J. H. Chu, C. T. Nelson, L. You, E. Arenholz, S. Salahuddin, J. Fontcuberta, T. Jungwirth, and R. Ramesh, Nat. Mater. **13**, 367 (2014).
[2]T. Moriyama, N. Matsuzaki, K. J. Kim, I. Suzuki, T. Taniyama, and T. Ono, Appl. Phys. Lett. **107**, 122403 (2015).
[3]P. Wadley, B. Howells, J. Elezny, C. Andrews, V. Hills, R. P. Campion, V. Novak, K. Olejnik, F. Maccherozzi, S. S. Dhesi, S. Y. Martin, T. Wagner, J. Wunderlich, F. Freimuth, Y. Mokrousov, J. Kune, J. S. Chauhan, M. J. Grzybowski, A. W. Rushforth, K. W. Edmonds, B. L. Gallagher, and T. Jungwirth, Science **351**, 587 (2016).
[4]T. Moriyama, M. Kamiya, K. Oda, K. Tanaka, K. J. Kim, and T. Ono, Phys. Rev. Lett. **119**, 267204 (2017).
[5]T. Moriyama, W. Zhou, T. Seki, K. Takanashi, and T. Ono, Phys. Rev. Lett. **121**, 167202 (2018).
[6]X. Z. Chen, R. Zarzuela, J. Zhang, C. Song, X. F. Zhou, G. Y. Shi, F. Li, H. A. Zhou, W. J. Jiang, F. Pan, and Y. Tserkovnyak, Phys. Rev. Lett. **120**, 207204 (2018).
[7]T. Moriyama, K. Oda, T. Ohkochi, M. Kimata, and T. Ono, Sci. Rep. **8**, 14167 (2018).
[8]H. Wang, C. Du, P. C. Hammel, and F. Yang, Phys. Rev. Lett. **113**, 097202 (2014).
[9]T. Moriyama, S. Takei, M. Nagata, Y. Yoshimura, N. Matsuzaki, T. Terashima, Y. Tserkovnyak, and T. Ono, Appl. Phys. Lett. **106**, 162406 (2015).
[10]C. Hahn, G. Loubens, V. V. Naletov, J. B. Youssef, O. Klein, and M. Viret, Europhys. Lett. **108**, 57005 (2014).
[11]T. Jungwirth, X. Marti, P. Wadley, and J. Wunderlich, Nat. Nanotechnol. **11**, 231 (2016).
[12]V. Baltz, A. Manchon, M. Tsoi, T. Moriyama, T. Ono, and Y. Tserkovnyak, Rev. Mod. Phys. **90**, 015005 (2018).
[13]R. Zhang and R. F. Willis, Phys. Rev. Lett. **86**, 2665 (2001).
[14]M. Farle, K. Baberschke, U. Stetter, A. Aspelmeier, and F. Gerhardter, Phys. Rev. B **47**, 11571(R) (1993).
[15]T. Ambrose and C. L. Chien, Phys. Rev. Lett. **76**, 1743 (1996).
[16]K. M. Kojima, Y. Fudamoto, M. Larkin, G. M. Luke, J. Merrin, B. Nachumi, Y. J. Uemura, N. Motoyama, H. Eisaki, S. Uchida, K. Yamada, Y. Endoh, S. Hosoya, B. J. Sternlieb, and G. Shirane, Phys. Rev. Lett. **78**, 1787 (1997).
[17]C. Niedermayer, C. Bernhard, T. Blasius, A. Golnik, A. Moodenbaugh, and J. I. Budnick, Phys. Rev. Lett. **80**, 3843 (1998).
[18]S. K. Sinha, J. W. Lynn, T. E. Grigereit, Z. Hossain, L. C. Gupta, R. Nagarajan, and C. Godart, Phys. Rev. B **51**, 681 (1995).
[19]J. Stöhr, A. Scholl, T. J. Regan, S. Anders, J. Lüning, M. R. Scheinfein, H. A. Padmore, and R. L. White, Phys. Rev. Lett. **83**, 1862 (1999).
[20]A. Scholl, J. Sto, J. Lu, J. W. Seo, J. Fompeyrine, H. Siegwart, J. Locquet, F. Nolting, S. Anders, E. E. Fullerton, M. R. Scheinfein, and H. A. Padmore, Science **287**, 1014 (2000).
[21]G. R. Hoogeboom, A. Aqeel, T. Kuschel, T. T. M. Palstra, and B. J. van Wees, Appl. Phys. Lett. **111**, 052409 (2017).
[22]L. Baldrati, A. Ross, T. Niizeki, C. Schneider, R. Ramos, J. Cramer, O. Gomonay, M. Filianina, T. Savchenko, D. Heinze, A. Kleibert, E. Saitoh, J. Sinova, and M. Kläui, Phys. Rev. B **98**, 024422 (2018).
[23]Y. Ji, J. Miao, K. K. Meng, Z. Y. Ren, B. W. Dong, X. G. Xu, Y. Wu, and Y. Jiang, Appl. Phys. Lett. **110**, 262401 (2017).
[24]R. Schlitz, T. Kosub, A. Thomas, S. Fabretti, K. Nielsch, D. Makarov, and S. T. B. Goennenwein, Appl. Phys. Lett. **112**, 132401 (2018).
[25]H. Nakayama, M. Althammer, Y.-T. Chen, K. Uchida, Y. Kajiwara, D. Kikuchi, T. Ohtani, S. Geprägs, M. Opel, S. Takahashi, R. Gross, G. E. W. Bauer, S. T. B. Goennenwein, and E. Saitoh, Phys. Rev. Lett. **110**, 206601 (2013).
[26]Y. T. Chen, S. Takahashi, H. Nakayama, M. Althammer, S. Goennenwein, E. Saitoh, and G. Bauer, Phys. Rev. B **87**, 144411 (2013).
[27]Y. Shiratsuchi, Y. Nakano, N. Inami, T. Ueno, K. Ono, R. Kumai, R. Sagayama, and R. Nakatani, J. Appl. Phys. **123**, 103903 (2018).
[28]S. Foner, Phys. Rev. **130**, 183 (1963).
[29]S. Foner and S. L. Hou, J. Appl. Phys. **33**, 1289 (1962).
[30]T. Kosub, M. Kopte, F. Radu, O. G. Schmidt, and D. Makarov, Phys. Rev. Lett. **115**, 097201 (2015).
[31]Y. Kota, H. Imamura, and M. Sasaki, Appl. Phys. Express **6**, 113007 (2013).